Meccanica **29:** 61–80, 1994.

Dynamics of Aerospace Vehicles at Very High Altitudes

NICOLA DE DIVITIIS, GUIDO DE MATTEIS and LUCIANO M. DE SOCIO
Università di Roma 'La Sapienza', Dipartimento di Meccanica e Aeronautica, via Eudossiana, 18, 00184 Roma, Italy

(Received: 26 June 1992; accepted in revised form: 18 February 1993)

Abstract. Some basic questions of the flight mechanics of aerospace vehicles at very high altitudes are investigated and in some cases reviewed. In particular those tracts of the spacecraft trajectories are considered along which the aerodynamic actions take place in a range of the Knudsen number between transition and free molecular flow. A recent physico–mathematical model is adopted in the evaluation of the aerodynamic and heat transfer coefficients. The stability characteristics are discussed of two reference vehicle configurations for which the time histories are also calculated relative to significant equilibrium conditions. In the final section of the paper the initial step of an aeroassisted orbit transfer is considered in order to evaluate the constraints due to the aerodynamic heating on this manoeuvre.

Sommario. Si studiano alcune questioni fondamentali della meccanica del volo di veicoli aerospaziali a quote molto elevate. Si considerano, in particolare, quei tratti delle traiettorie lungo i quali le azioni aerodinamiche si esplicano in un campo di numeri di Knudsen tra la transizione ed i flussi di molecole libere. Si adotta un recente modello fisico-matematico per calcolare i coefficienti aerodinamici e di scambio termico. Dopo aver discusso le caratteristiche di stabilità per due configurazioni di velivoli di riferimento, se ne calcolano le leggi orarie a partire da condizioni di equilibrio significative. Il lavoro termina con lo studio di un trasferimento orbitale aeroassistito al fine di valutare i limiti a questa manovra dovuti al riscaldamento aerodinamico.

Key words: Flight dynamics, aerospace vehicles, aircraft dynamics.

Nomenclature

c_h	local heat transfer coefficient
c_n, c_t	normal and tangential local force coefficients
C_D, C_L	drag and lift coefficients
C_M	longitudinal moment coefficient
C_H	heat transfer coefficient
D	drag force
E	aerodynamic efficiency $= C_L/C_D$
f	distribution function
F_x, F_z	thrust force components
g	acceleration of gravity
$\dot{h}$	mean heat transfer rate
H	altitude
Kn	Knudsen number
I_x, I_y, I_z	moments of inertia
l	free molecular path
L	lift force
ℓ	characteristic length

m	mass
M	Mach number
M_{aer}	aerodynamic moment
M_g	gravitational moment
M_{trim}	trim moment
q	pitch rate
$\mathfrak{R}$	geocentric radius
s	speed ratio
S	reference surface
t	time
T_0	stagnation temperature
T_W	wall temperature
u, w	velocity components
u_{orb}	circular orbital velocity $= (g\mathfrak{R})^{1/2}$
x, z	Cartesian body axes
X, Z	aerodynamic force components

Greek symbols

α	angle of attack
γ	ratio of the specific heats
δ	local incidence
θ	pitch angle
λ	eigenvalue
μ	mass ratio
ρ	density
τ_W	temperature ratio $= T_W/T_0$
ω^E	Earth angular velocity
ω_{orb}	circular orbital frequency

Superscripts

$'$	perturbation value

Subscripts

e	equilibrium
FMF	free molecular flow
g	geometric
∞	at infinity

1. Introduction

Flight at very high altitudes, in the region which is usually thought of as the border of the atmosphere, presents some peculiar aspects. Here the density of the air has decreased to the point that the length of the molecular free path, l, becomes more and more comparable with a characteristic linear dimension, ℓ, of a manned vehicle. The speed of a body has, of course, to be very high in order to determine sizeable lifting effects and the aerodynamics of the vehicle is then governed by the laws of rarefied gasdynamics and the assumption of hypersonic conditions is very likely to be verified.

A great variety of either realized or proposed aerospace objects moves in the atmospheric layer where the Knudsen number, $\mathrm{Kn} = l/\ell$, falls in the interval $(0.01–\infty)$. This interval corresponds to regimes from the slip flow through the transition to the free molecular flow. One can deal with the slip flow field practically by the same techniques adopted for the continuous flow regime, facing the same difficulties, provided that the proper boundary conditions are taken into account in the differential problem. On the other extreme of the interval, free molecular flows have been thoroughly investigated and a great deal of applicable results are available for the study of the aerodynamic actions on lifting bodies. The wide range of transitional flows, say between $\mathrm{Kn} = 0.05$ and $\mathrm{Kn} = 1$, still presents extreme difficulties to be surmounted either theoretically and experimentally before really satisfactory computational procedures are available. In this respect, from the engineering point of view, promising results have been shown by the main versions and modifications of the Monte Carlo Simulation Numerical Methods (MCDS) [1, 2], although their implementation is in any case burdensome for complicated geometries.

As for the vehicles, the performances of which take place in the transitional regime, we cite only the shuttle-type spacecraft (STS), the Hermes project, the personnel launch vehicles (PLV), the manoeuvrable re-entry research vehicles (MRRV), the aeroassisted orbital transfer vehicles (AOTV), the downward deployed tethered satellite where it is aerodynamically controlled and the space transport modules, etc. [3].

In this paper we will consider two of the main areas of the flight dynamics of lifting vehicles in the upper atmosphere, namely the stability of the equilibrium and the flight performances in a typical mission. Considerable research from the 1950s has been in the first area and its familiar background formulation is reported in a renown textbook by Etkin [4]. The second one has been investigated more recently with additions changing from time to time according to the specific mission profiles of the vehicles. Our contribution is essentially founded on the adoption of a new, accurate model for the aerodynamic interaction and heat transfer between a transitional rarefied gas flow and a solid wall [5]. This model is simple enough to be applied with ease and enables the problem of stability to be reviewed, thus reaching much more realistic conclusions with respect to the rough first approximation. This is particularly true if one considers that the aerodynamic behaviour of a lifting body is usually non-linear. Because of this, it seemed appropriate to substantiate the results of a linear stability procedure with those of the solution to the full set of governing equations. The second step is then to take advantage of the capabilities of the model in evaluating and discussing the performances of lifting spacecraft at very high altitudes.

In many previous works it is quite customary to assume that beyond a limit of, say, 100 or 110 km above the Earth, aerodynamic actions are vanishingly small [6]. Apart from the fact that this statement is not true in all circumstances, problems which involve the stability of equilibrium can indeed be strongly affected by the aerodynamic forces and moments.

Furthermore the choice of the model for the gas–surface interaction can play a great role. As an example we recall that, in most cases, at high Kn, the lift and drag coefficients, namely C_L and C_D, can be adequately predicted within a free molecular flow approximation. However, the heat transfer coefficient C_H cannot. On the other hand, for finite although great values of Kn, C_L and C_D depend on the thermal exchanges at the walls. Therefore, even in the case of small values of C_L and C_D in some tracts of a mission, the value of C_H can be sufficient to change the thermal conditions of the vehicle and influence future parts of its trajectory. This leads to the second phase of this research where we carry out an investigation of a significant mission which begins from an initial orbit of equilibrium and proceeds towards denser layers of the atmosphere while limitations due to the aerodynamic heating intervene in the decision of the proper course. Attention is also paid to previously adopted physico–mathematical models of the gas–surface interactions.

In short, we will show that an appropriate consideration of the aerodynamic forces and moments and of the heat transfer in those regions where they are either neglected or incorrectly evaluated can result in a more advanced analysis of the possible performances and stability of spacecraft.

A note before ending this introduction. From the aerodynamic point of view of the load-evaluation, response to controls and convective heat transfer, there is still the open question of how to manage the density potholes in the sky adequately. These are regions where the number of particles per unit volume can change at random of even one order of magnitude from time to time. In this respect a better approach to the problem may be found in a stochastic simulation of the physical characteristics of the atmosphere [7]. Here we will stay on the much more usual deterministic foundations, while keeping in mind how cautious the investigator should be when presenting his or her results connected with the atmospheric actions at high altitudes. As a further hypothesis we will assume that the low density plasma effects of the ionospheric regions can be neglected.

2. Aero-Thermodynamic Coefficients

In a recent work a physico–mathematical model was presented which is able to correctly predict functional relations for the momentum and energy transfer between a rarefied gas stream and a solid surface [5]. The model is based on a *boundary layer* assumption which is adopted for the approximate description of the distribution function f in a Knudsen layer. We will not go too deeply into details in this paper and will limit the presentation to a summary of the main aspects of the model.

After expressing the Boltzmann equation in non-dimensional form, the space derivatives of f in a direction tangent to the layer are neglected with respect to the normal derivative. The resulting *boundary layer* simplification of the Boltzmann equation can subsequently be analytically integrated under some further hypotheses on the molecular collision frequency distribution in the layer and upon the law of reflection from the wall. This leads to relations of the kind which follows for the area element at an incidence δ

$$\left.\begin{aligned} c_n(\delta, \tau_W, \mathrm{Kn}_\infty) &= [c_{p_{FMF}}(\delta, \tau_W)]\phi_1(\mathrm{Kn}_\infty, \delta) \\ c_t(\delta, \mathrm{Kn}_\infty) &= [c_{t_{FMF}}(\delta)]\phi_2(\mathrm{Kn}_\infty, \delta) \\ c_h(\delta, \tau_W, \mathrm{Kn}_\infty) &= [c_{h_{FMF}}(\delta, \tau_W)]\phi_3(\mathrm{Kn}_\infty, \delta) \end{aligned}\right\} \tag{1}$$

where the expressions in free molecular flow (FMF) of the normal and tangential aerodynamic forces and of the heat transfer coefficient are

$$\left.\begin{aligned} c_{n_{FMF}} &= 2\sin\alpha(\sin\alpha + \beta\eta) \\ c_{t_{FMF}} &= 2\sin\alpha\cos\alpha \\ c_{h_{FMF}} &= (1 - \beta^2\eta^{3/2})\sin\alpha \end{aligned}\right\} \tag{2}$$

and

$$\phi_i = A_i + (1 - A_i)\exp(-a_i \sin\alpha/\mathrm{Kn}_\infty)\,, i = 1, 2, 3 \tag{3}$$

where $\eta = [(\gamma - 1)/\gamma]^2$, with γ being the ratio of the specific heats. In the equations for ϕ_i, the parameters A_i and a_i, which depend upon the species of gas, were identified through comparisons with the experimental data obtained in DVRL Göttingen Laboratories [8]. Note that the aerodynamic coefficients depend on the aerodynamic local incidence δ, on the ratio $\tau_W = T_W/T_0$ between the wall temperature and the stagnation temperature of the stream and on the Knudsen number, Kn_∞. Furthermore, $\beta = \beta(\tau_W) = [0.5\tau_W(1 + \gamma)\gamma^2/(\gamma - 1)^3]^{1/2}$.

The expressions above are the result of a hypersonic approximation in the sense that they represent the limit, for the Mach number M_∞ tending to infinity, of more general relations, which can be found in [5], where the generic coefficient is a function of α, τ_W, Kn_∞ and M_∞. This hypersonic approximation introduces negligible errors in the applications which will be presented, where the Mach number at infinity exceeds 18.

From Equations (1) the lift, drag, moment and total heat transfer coefficients, namely C_L, C_D, C_M and C_H, can be easily evaluated by integration over all the vehicle surface with the exception of the regions in shadow. A procedure similar to the one which we have summarized also leads to the expressions of the aero-thermodynamic coefficients in unsteady situations. Here we will use the steady aerodynamic derivatives only (in particular the moment derivative $\partial C_M/\partial\alpha$) since it can be shown that the unsteady corrections are very small in the cases investigated [5].

With respect to the results of the Newtonian theory, the hypersonic continuum theory and of the theory of free molecular flows, the model described covers more appropriately the range of Knudsen numbers which fall in the transition regime, since it assumes a diffuse reflection of the particles from the wall. From the experiments and from the theory of transitional flow the heat transfer coefficient C_H vanishes as $\mathrm{Kn}_\infty \to 0$. Therefore one knows that the heat transfer rate at decreasing altitudes initially increases since the density is increasing more rapidly than the decrease of Kn_∞ and then decreases. This puts an altitude limit to the validity of the model at least as a means of predicting the heat transfer characteristics. On the other hand we observe that if we used the free molecular theory or the Newtonian theory, where the particles are specularly reflected from the wall surface, we would arrive at the prediction that the heat transfer rate is zero. In addition we notice that our results mismatch to an order of magnitude the relation which is shown in [9] for the heat transfer in continuum flow, at an altitude of 110 km, where the customary border of a vanishingly dense atmosphere is located. But we will also see that the model leads to an evaluation of the aerodynamic coefficients which can be extended well down to relatively low altitudes in very good agreement with the existing theories for low Kn.

Here we address the reader to the next section where the aerodynamic characteristics of two sample spacecraft will be presented. There one will note, as an example, that the efficiency

Table 1. Dimensions and mass

Length, m	8.61
Wing span, m	4.65
Planform area, m^2	26.6
Mass, kg	8652
I_x, kg m^2	10184
I_y, kg m^2	45553
I_z, kg m^2	48322

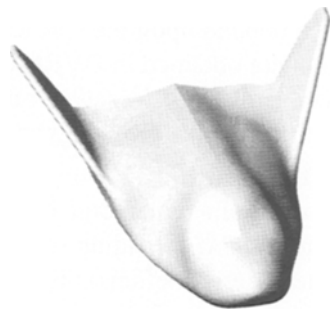

Fig. 1. A proposed personnel launch vehicle (PLV).

$E = C_L/C_D$ changes with Kn_∞ at fixed angle of attack α and τ_W in front of the constant value in free molecular flow ($\mathrm{Kn}_\infty \to \infty$).

All the calculations in this paper were carried out adopting the U.S. Standard Atmosphere [10].

3. The Reference Vehicles

As described, we chose two very different geometric configurations as reference vehicles with which to explore a wide range of possible dynamic behaviours. Figures 1 and 2 show the considered geometries and Table 1 provides some further information. The total mass, the moments of inertia and the reference area are, in both cases, the same in order to demonstrate the influence of the aerodynamic factors. Figure 1 presents a sketch of a proposed PLV [11] and a non-conventional aircraft shaped as a Nonweiller's *caret* wing waverider [12, 13] is shown in Figure 2.

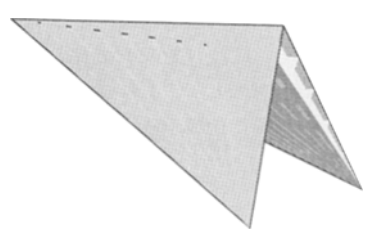

Fig. 2. A caret wing waverider (Nonweiller).

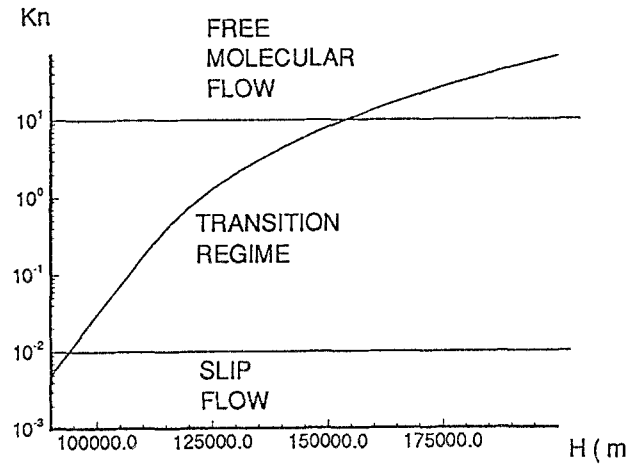

Fig. 3. Reference Knudsen number versus altitude H (reference length $\ell = 8.61$ m).

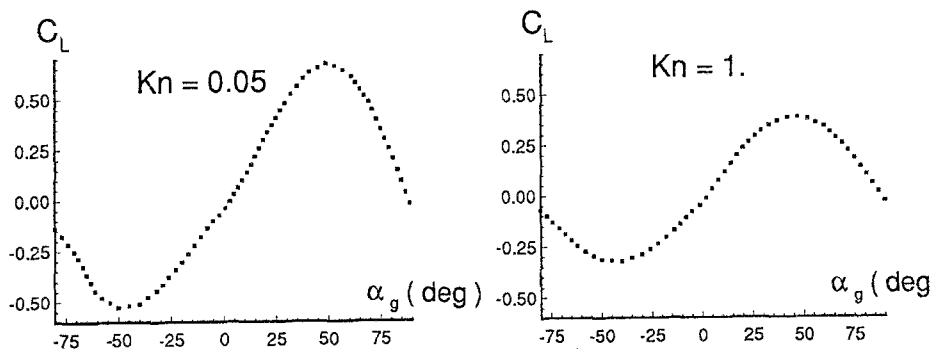

Fig. 4. Lift coefficient versus α at $\tau_W = 1$ for the PLV.

The curves which give the aerodynamic coefficients, the efficiency and the heat transfer coefficient as functions of the angle of attack, of the Knudsen number and of the temperature ratio were calculated according to the transition flow model introduced.

For both spacecraft we assumed a reference length in the Knudsen number evaluation equal to the overall length $\ell = 8.61$ m. The curve in Figure 3 which represents Kn_∞ versus the altitude H, will then be useful as a quick reference. Also shown are the conventional bounds of the flow regimes.

Figures 4 and 6–9 give the basic coefficients for the vehicle shown in Figure 1. In particular Figure 4 shows the variations of the lift coefficient versus the aerodynamic angle of attack for two different values of Kn_∞ and for $\tau_W = 1$. From our calculations we note that the zero lift direction of the PLV changes of a few tenths of one degree in the entire range of Kn_∞ and for $0 \leq \tau_W \leq 1$. For the caret wing the changes are even smaller, (see Figure 5). Figure 6 reports the aerodynamic efficiency which undergoes great variations with Kn_∞. The moment coefficient versus α is represented in Figure 7 for two values of Kn_∞ at $\tau_W = 1$. Similarly, Figure 8 shows the great variations of C_H.

The influence of the temperature ratio can be realized if one considers Figure 9 which shows C_M and C_H in two extreme situations, $\tau_W = 0$ and $\tau_W = 1$ respectively, in free molecular flow ($\mathrm{Kn}_\infty = 10$). Note that for the particular examples which will be dealt with,

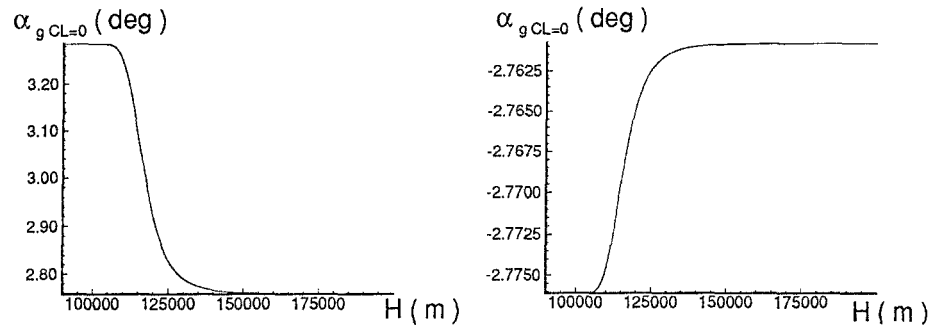

Fig. 5. Zero lift angle versus altitude H for the PLV (left) and the caret wing spacecraft (right).

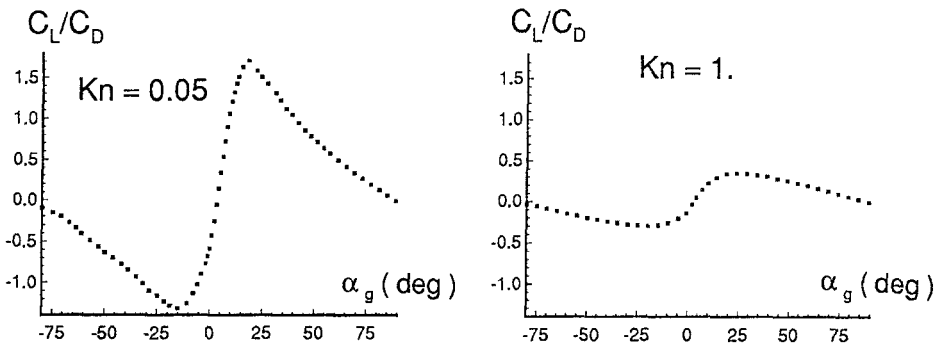

Fig. 6. Aerodynamic efficiency versus α at $\tau_W = 1$ for the PLV.

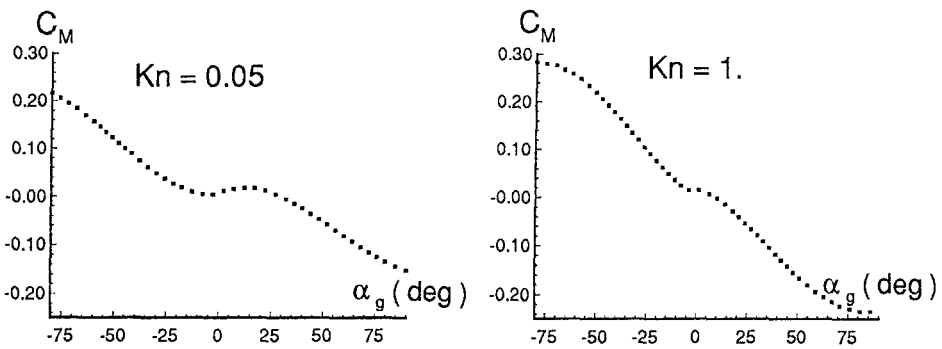

Fig. 7. Moment coefficient versus α at $\tau_W = 1$ for the PLV.

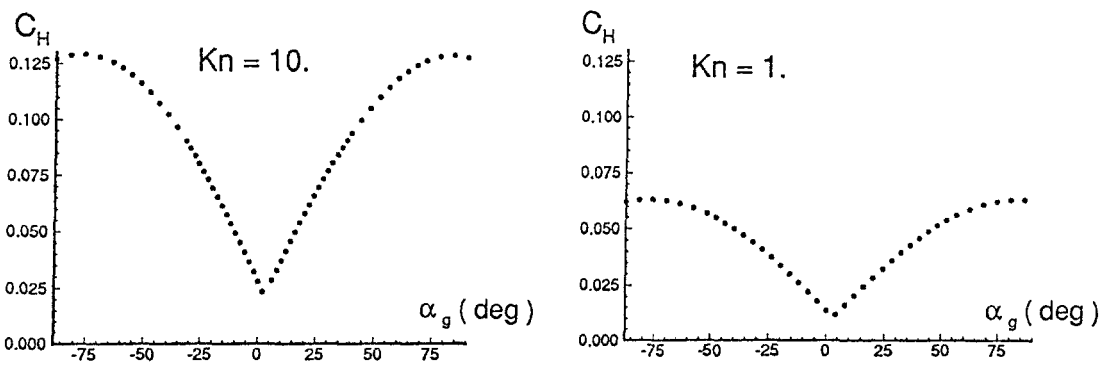

Fig. 8. Heat transfer coefficient versus α at $\tau_W = 1$ for the PLV.

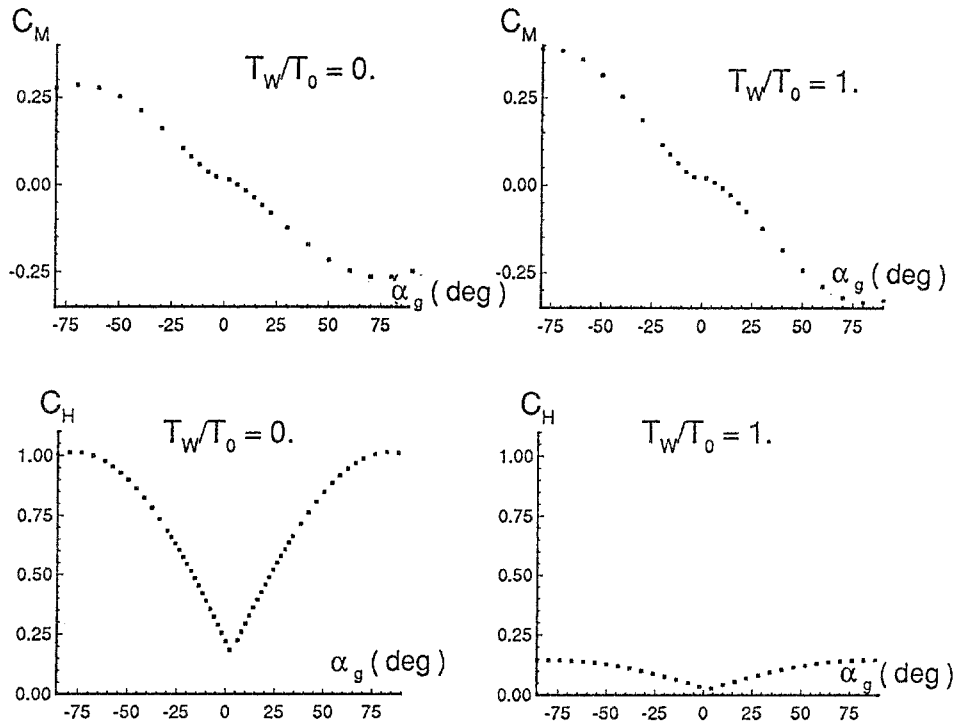

Fig. 9. Influence of the temperature ratio on the moment coefficient and on the heat transfer coefficient for the PLV at $\mathrm{Kn}_\infty = 10$.

conditions of practical heating limitations will always involve values of τ_W which are very small [14].

When the caret wing configuration is considered the same general trends can be observed.

It is important to consider the relatively high values of the coefficient of the moment around the centre of gravity and the fact that the moment derivative with respect to α can change sign at some α. This last fact can determine unfavourable stability characteristics of the spacecraft, as we will see later. However, the current problem is: Is it possible to design practical spacecraft geometries for which the values $\partial C_M/\partial\alpha$ are negative in such an extended range of incidences so to cover all the possible flight conditions? In this question we refer to flight corridors where the Knudsen numbers change from the free molecular to the slip flow regimes. The answer is to be found in a still open field of investigation. In this respect we think that this problem should be associated with those researches concerning the optimization of the shape of the spacecraft from the point of view of drag, efficiency and heat transfer which are in constant development.

We can finally compare some of our results with recently published data. Anderson *et al.* [13] used Potter's bridging formulae [15, 16] to evaluate the characteristics of their viscous optimized waveriders, and Powell *et al.* [11] adopted an Aerodynamic Preliminary Analysis System (APAS) [17]. Both Potter's formulae and the APAS rely on correlations of experimental (wind tunnel and STS) and analytical and numerical (MCDS) data. As such the results of these interpolated expressions only give more or less accurate approximations of the relevant global aerodynamic and heat transfer characteristics of complex bodies. More accurate results are apparently those obtained by similar procedures in the work at the TsAGI (Central Aero-Hydrodynamical Institute) in Moscow [18].

These approximations become more and more a matter of discussion as one moves from continuum towards the transitional regime. Although the shape of the vehicles examined in [11,13] is not the shape of a Nonweiller caret configuration, we recall that in rarefied gas flow the most important geometric parameters of waverider spacecraft of moderate thickness are the planform and the angle of attack [19]. A very rough explanation of this rule is the fact that in rarefied gas dynamics the most effective area, as far as the aerodynamic action is concerned, is that of the projection of the whole spacecraft surface normal to the approaching stream. In this context the PLV, which is considered here, has a maximum percental thickness equal to 0.22. When we compare our data with those in [13] we obtain the following results for the maximum efficiency as a function of the altitude $E_{\max} = E_{\max}(H)$: $E_{\max} = 1.75$ and 0.37 at $H = 80$ and 120 km, respectively, instead of 1.71 and 0.36 at the same values of H as reported in [13]. We see that our model is still accurate in evaluating E at relatively low altitudes.

Above the atmospheric border the only solution method in the existing literature which would provide satisfactory calculations of the aero-thermodynamic coefficients is that of MCDS. However, its application is cumbersome and computer time consuming with respect to our model.

4. Fundamental Equations and Stability Analysis

In the following we will consider, for the sake of simplicity, motions in the equatorial plane of the Earth. The atmosphere rotates rigidly with a spherical Earth. The fundamental governing equations are then [4]

$$\begin{aligned} m\dot{u} &= -m(q-\omega^E)w - mg\sin\theta + X + F_x \\ m\dot{w} &= m(q-\omega^E)u + mg\cos\theta + Z + F_z \\ I_y\dot{q} &= M_{\text{aer}} + M_g + M_{\text{trim}} \\ \dot{\theta} &= q + \omega^E + (u\cos\theta + w\sin\theta)/\mathfrak{R} \\ \dot{\mathfrak{R}} &= u\sin\theta - w\cos\theta \end{aligned} \tag{4}$$

where M_{aer} and M_g are the aerodynamic and gravitational moments respectively, and M_{trim} is the trim moment which is due to the action of thrusters. The meaning of the other symbols is reported in the Nomenclature.

If we consider as the initial state of the vehicle the one corresponding to a steady circular orbit, then the equilibrium equations are, in stability axes,

$$\begin{aligned} F_{x_e} - D_e &= 0 \\ m(q_e-\omega^E)u_e - L_e + F_{z_e} + mg &= 0 \\ q_e + \omega^E + u_e/\mathfrak{R}_e &= 0 \\ M_{g_e} + M_{\text{aer}_e} + M_{\text{trim}} &= 0 \end{aligned} \tag{5}$$

The equilibrium solution is computed, after assuming $F_z = 0$, by assigning the geocentric radius $\mathfrak{R}_e$ and the angle of attack of the vehicle, and determining q_e, u_e, M_{trim} and F_{x_e}. As usual, we used the inverse square law for g and the following relation for the gravitational moment [4]

$$M_g = -\frac{3}{2}\frac{g_e}{\mathfrak{R}_e}(I_x - I_z)\sin 2\theta.$$

Finally, the linearization procedure yields the following equations for the state $\mathbf{x}^T = (u', w', \theta', \mathfrak{R}', q')$ in fixed control conditions

$$
\begin{aligned}
\dot{u}' &= -\frac{\rho_e u_e S C_{D_e}}{m} u' - \left(q_e - \omega^E + \frac{\rho_e u_e S}{2m} \left. \frac{\partial C_D}{\partial \alpha} \right|_e \right) w' - g_e \theta' - \frac{\rho_e u_e^2 S C_{D_e} \Lambda}{2m} \\
&\quad \times \left(1 - \frac{1}{C_{D_e}} \left. \frac{\partial C_D}{\partial \mathrm{Kn}} \right|_e \mathrm{Kn}_\infty \right) \mathfrak{R}' \\
\dot{w}' &= \left(q_e - \omega^E - \frac{\rho_e u_e S C_{L_e}}{m} \right) u' - \frac{\rho_e u_e S}{2m} \left. \frac{\partial C_L}{\partial \alpha} \right|_e w' \\
&\quad - \left[\frac{\rho_e u_e^2 S C_{L_e} \Lambda}{2m} \left(1 - \frac{1}{C_{L_e}} \left. \frac{\partial C_L}{\partial \mathrm{Kn}} \right|_e \mathrm{Kn}_\infty \right) + 2 \frac{g_e}{\mathfrak{R}_e} \right] \mathfrak{R}' + u_e q' \qquad (6) \\
\dot{\theta}' &= \frac{1}{\mathfrak{R}_e} u' + \frac{q_e + \omega^E}{\mathfrak{R}_e} \mathfrak{R}' + q' \\
\dot{\mathfrak{R}}' &= -w' + u_e \theta' \\
\dot{q}' &= \frac{\rho_e u_e \ell S C_{M_e}}{I_y} u' + \frac{\rho_e u_e \ell S}{2 I_y} \left. \frac{\partial C_M}{\partial \alpha} \right|_e w' - \left(3 \frac{g_e}{\mathfrak{R}_e} \frac{I_x - I_z}{I_y} \cos 2\theta_e \right) \theta' \\
&\quad + \frac{\rho_e u_e^2 \ell S C_{M_e} \Lambda}{2 I_y} \times \left(1 - \frac{1}{C_{M_e}} \left. \frac{\partial C_M}{\partial \mathrm{Kn}} \right|_e \mathrm{Kn}_\infty \right) \mathfrak{R}'
\end{aligned}
$$

where $\Lambda = \left(\partial \rho / \partial \mathfrak{R}\right)_e / \rho_e$ and the aerodynamic coefficients C_L, C_D and C_M are defined as in [4], when taking into account that the reference area S is the total area of the planform of the spacecraft.

When the eigenvalues of the state matrix are sought, the linear stability characteristics of the aerospace vehicle can be determined. Like the more or less conventional airplanes, in our present case we can distinguish those among the roots of the characteristic equation which can be referred to as the short period mode and the phugoid. Furthermore a height mode which corresponds to a fifth real root is present.

As we have already observed, care must be taken when dealing with the results of the linearization procedure. This fact can be immediately realized by sheer observation of the behaviour of the aerodynamic coefficients (Figures. 4–9) and after considering that the range of the angles of attack which may be required along some portions of the flight path can, for various reasons, be very large.

For a discussion of the equilibrium condition on a circular orbit we recall the definition of the speed ratio $s = (u_e + \mathfrak{R}_e \omega_e)/u_{\mathrm{orb}}$ where u_{orb} is the circular orbit velocity. For $C_{L_e} = 0$ one has $s = 1$, for $C_{L_e} > 0$ the flight is at subcircular speed and $s < 1$, and for $C_{L_e} < 0$ the flight is at supercircular speed and $s > 1$.

It is easy to show that the angle of attack of minimum drag in equilibrium α_{opt} is given by the minimum value of

$$C^* = C_D/(1 + C_L/2\mu) \qquad (7)$$

with $\mu = m/\rho S \mathfrak{R}_e$. Obviously, to the minimum fuel consumption corresponds C^*_{min} and $s < 1$, for $C_L > 0$.

Figure 10 shows the angles of attack of minimum drag and the corresponding efficiencies as functions of the altitude for the two reference vehicles.

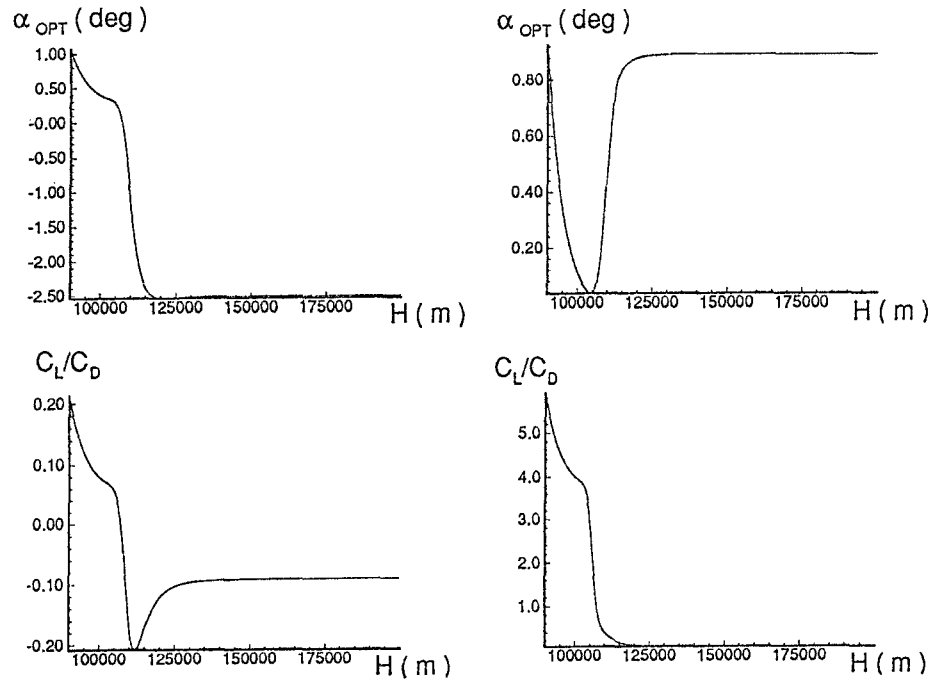

Fig. 10. Angle of attack of minimum fuel consumption and corresponding efficiency versus altitude for $\tau_W = 1$. PLV(left), caret wing configuration (right).

In Figure 11 the root loci are represented for the PLV at three different angles of attack. The first case corresponds to a very small incidence, the second one to $C_{L_{\max}}$ and the third case to an incidence very close to that for which the aerodynamic derivative $\partial C_M/\partial\alpha$ changes its sign from negative to positive. Note that in all these cases the aerodynamic angle of attack is changing with the altitude since the incidence of zero lift changes.

Similar curves can be obtained for the caret wing configuration, at least as far as the qualitative behaviour is concerned.

Before going into detail we point out that a comparison of our results with those obtained by Etkin shows many similarities and a few striking differences. The reason for this lies on the choice of an almost conventional plane outlined in [4, 6]. This choice obviously has a very great influence on the moments of inertia. Furthermore the polar curve in the previous examples follows a hypersonic Newtonian relationship and, most important, the aerodynamic moment derivative with respect to the angle of attack, $\partial C_M/\partial\alpha$, is supposed to be constant and negative in all circumstances. This last assumption leads to a much more favourable although not too realistic conclusions on the stability of the spacecraft.

When we consider Figure 11 we note that the so called height mode is always a positive real root, the value of which increases with the angle of attack. Depending on the sign of the perturbation, the spacecraft leaves from its initial orbit and steadily either increases or decreases its altitude, apart from the other superimposed modes of this linear approximation. But the phugoid is stable in the three cases and is more or less damped, the damping factor depending on the incidence and on the altitude. At about 120 km its frequency is practically undistinguishable from the orbital frequency in any case.

The root locus of what we conventionally still call the short period mode is very interesting. Such a mode corresponds to a periodic not amplified motion in a finite range of H for small

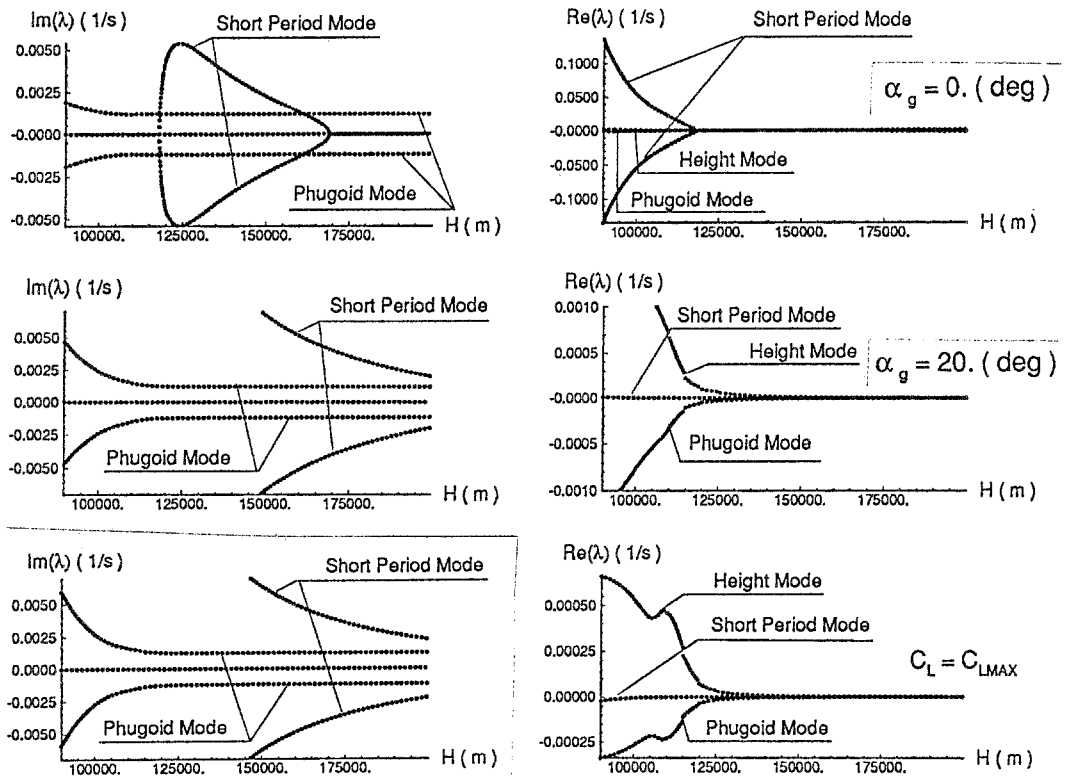

Fig. 11. Root locus versus altitude for the PLV, $\tau_W = 1$; $\alpha_g = 0°$ (top), $\alpha_g = 20°$ (middle), $\alpha_g(C_{L_{\max}})$ (bottom).

angles of attack α_g. In this range its frequency can show two crossovers of the phugoid frequency, the altitude at which this happens depending on α_g. In particular, where α_g is not too small, the short period mode is always periodic and not amplified.

The presence of a cross-over frequency has been observed by Etkin in a very peculiar case [4]. Here we note that this is not a general rule. Above and below the limit values of H for a short period motion to exist we have a degeneracy of conjugate complex roots which yields two real roots, one of which corresponds to an unstable amplified aperiodic motion. The absolute values of the amplification and the damping factors are relatively great at lower H. When greater angles of attack are considered the short period mode is always unstable but its influence on the trajectory becomes negligible at upper altitudes.

As we said, analogous results can be obtained for the spacecraft shown in Figure 2. The major difference is in the fact that the C_M versus α curve presents a range of positive slope more extended than in the case of the PLV.

5. Time Histories

In the preceding section we went through a linear stability analysis of the orbital equilibrium conditions for two extremely different aerodynamic configurations of an aerospace vehicle. We already recalled the limitations and the difficulties connected with the linearization procedure. Whenever possible, in the presence of these problems, a deeper investigation of the dynamic characteristics of the system should at least be associated with the computation of the time histories which follow significant perturbations of representative initial states.

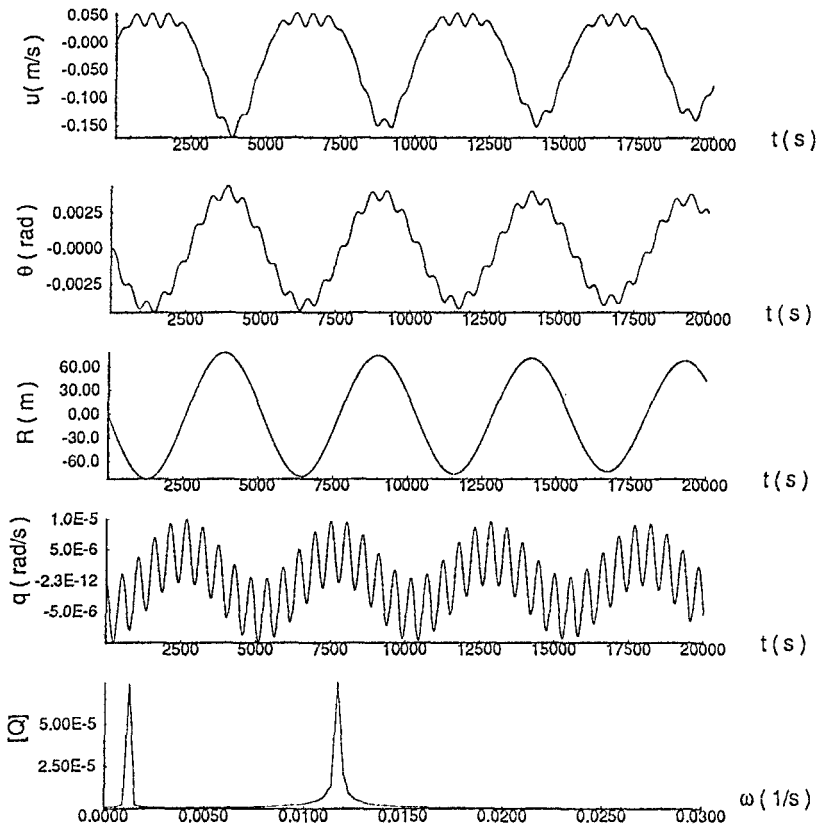

Fig. 12. Time history of the PLV, $\tau_W = 1$, at $\alpha_g(C_{L_{\max}})$, $H_e = 130$ km, $\Delta w = 0.1$ m s^{-1}.

For this reason we show, in Figures 12–14, the time histories of our two spacecraft after their initial orbital motions were perturbed. In both cases a variation of the vertical speed component of $\Delta w = 0.1$ ms^{-1} from the zero equilibrium value determines the changes of the main state variables which are represented over a time span of a few orbit periods.

Figure 12 shows that the linear approach to the stability analysis is still acceptable for the PLV in its subcircular flight at 130 km of altitude. As we said, the angle of attack, which in this case is kept equal to $\alpha_g(C_{L_{\max}})$, corresponds to an aerodynamic incidence changing with the variations of altitude during the perturbed motion. In contrast with the usual behaviour of aircraft in the continuous regime, flying at $C_{L_{\max}}$ is possible since the viscous separation and stall are not present in rarefied gas dynamics. In this last situation one only faces the separation related to the existence of shadowed regions which are always present for bodies of finite thickness.

When the spectral, fast Fourier transform (FFT) analysis is carried out of, say, variable q, then the bottom of Figure 12 gives the results in the frequency domain of the transform $[Q]$. The two peaks are centred around the values of the phugoid and the short period modes as obtained in the preceding section. At the altitudes considered the lower frequency is comparable with the frequency of the inertial orbital motion, $\omega_{\text{orb}} = 1.1 \times 10^{-4}$ s^{-1}.

In the example of Figure 12 the time history develops in a range of aerodynamic incidences to which negative values of the slope of the C_M curves as a function of α and Kn_∞ correspond.

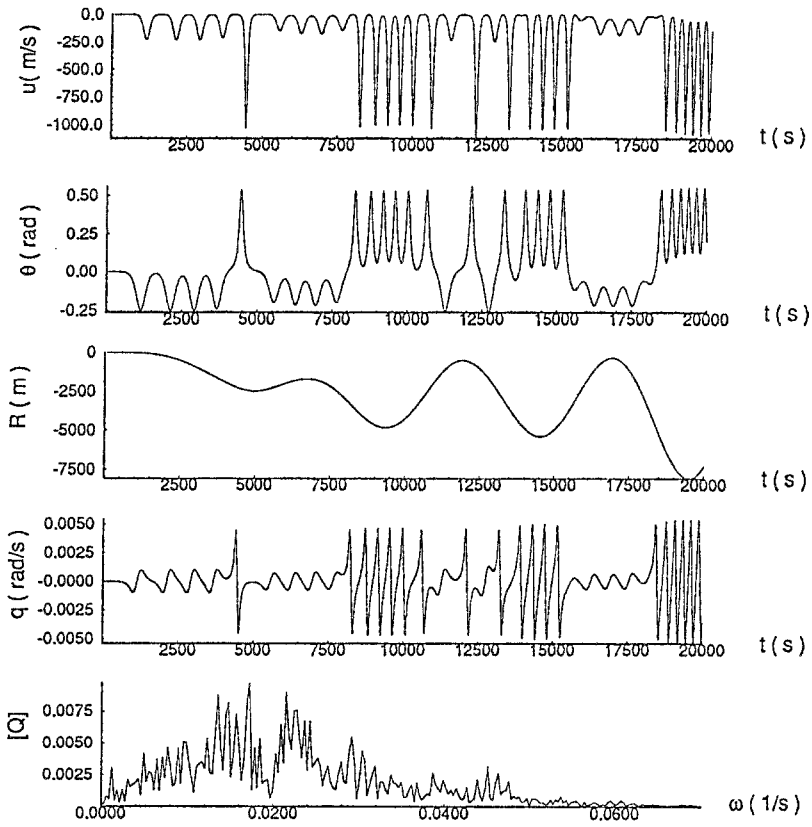

Fig. 13. Time history of the caret wing configuration at $\alpha_g = 20°$: $\tau_W = 1$, $H_i = 120$ km, $\Delta w = 0.1$ m s^{-1}.

In any case, note that the unstable height mode leads to a slow descent of the trajectory, since the initial thrust value is kept unchanged.

If we now consider the problem of a caret wing spacecraft, we assume initial equilibrium conditions such that the value of the derivative $\partial C_M/\partial\alpha$ is close to zero. In particular, we take $H_e = 120$ km, $\alpha_{g_e} = -10°$, and the same w speed variation as before. The perturbation determines the time history which is presented in Figure 13. In spite of the extremely low value of the initial perturbation the unstable equilibrium leads to results which could not be obtained by the linear stability analysis. The fact that this linear theory is not acceptable anymore is confirmed by observing the spectrum of $[Q]$. In the figures, for the sake of clear representation, the diagram of the w speed component is not reported since it practically follows the trend of the pitch angle variable.

It is meaningful to consider Figure 14 where the time histories of a significant state variable of the two spacecraft are shown in the phase plane. The results for the caret wing configuration correspond to the initial situation of Figure 13 as those for the PLV with the only exception that, in the second case, the initial incidence is $-2°$. Again, this last value was assumed in order to have a value of $\partial C_M/\partial\alpha$ at $t = 0$ close to zero. Both the trajectories in the phase plane are encircling two limit positions which slowly change with altitude and correspond to a vanishing value of C_M.

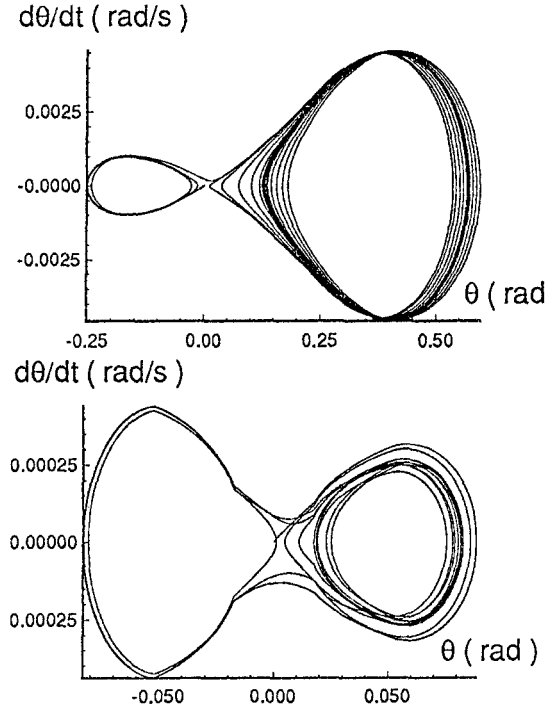

Fig. 14. Time histories in the phase plane of the caret wing spacecraft at $\alpha_g = 20°$ (top) and of the PLV at $\alpha_g = -2°$ (bottom): $\tau_W = 1$, $\Delta w = 0.1\ \mathrm{m\,s^{-1}}$, $H_e = 120\ \mathrm{km}$.

6. Manoeuvre of an AOTV

The time histories of the spacecraft in Section 5 were numerically obtained by realizing a simulation computer's code for solving the system of motion equations. The system is augmented by the equations which represent the physico–mathematical model for the gas–surface interactions. We will now use the same code for the solution of a problem which represents the second part of the research on the influence and correct evaluation of the atmospheric effects at very high altitudes on the spacecraft. Before proceeding any further a short foreword is necessary about the selected reference manoeuvre to be examined.

The synergistic plane change of an AOTV has received ever increasing attention in recent times for applications to vehicles around the Earth and other planets of the Sun. We will not concentrate too much on the many aspects of this complicated problem [20]. We simply enumerate the phases through which the vehicle changes the plane of its orbit.

As a first step the AOTV deorbits via a thrust impulse and through a parabolic or elliptic trajectory arrives at a new orbit at the edge of the atmosphere. The vehicle departs from this situation and through an aeroassisted descent mode and an aerocruise changes its heading. The final phases will be an aeroassisted ascent mode and the reorbit.

Until very recently [9] the studies relative to manoeuvres similar to the ones which we are describing have been essentially based on a somewhat arbitrary definition of a limit altitude above which the aerothermodynamic effects are practically negligible. As we have already seen, although this position may in principle be accepted when dealing with the determination of the aerodynamic forces, this no longer applies when stability problems are taken into account since even vanishingly small aerodynamic moment perturbations can be followed

by sizeable effects. Similar considerations can result concerning the importance of a correct evaluation of the heat transfer. From this evaluation, as we said, apart from better calculations of the aerodynamic coefficients, we obtain the heating history of the spacecraft with its effects on the structures and the cooling system.

We recall that in the AOTV manoeuvre, as in many other cases, strict limitations apply to fuel consumption, load factor, flight control capability and aerodynamic heating. What we will deal with in the sequel is related to the very sensitive point of the energy exchange between vehicle and stream from the point of view of the aerodynamic heating of the body. As is well known, and we already saw while presenting the model for the gas–solid interaction, in the transition regime even the aerodynamic coefficients depend on the temperature ratio τ_W.

To the authors' knowledge, all the previous calculations of the heating limits in this and similar problems, like that of the atmospheric re-entry, were carried out by taking into account the value of the maximum heat transfer rate for an assigned reference value of the maximum wall temperature. In this regard the Lees formula was frequently used [21] and, more recently, expressions such as those adopted in [9, 15, 16] have become popular. In our case we will use the analytic expressions of the heat transfer coefficient which allow for the calculation of both the local and the global heat transfer rates. For simplicity we will not consider the full problem of the energy balance of a spacecraft where gains in the form of convection heat are dissipated by losses through a radiation process. Furthermore we will suppose that the wall is kept at the usual reference maximum temperature of 1.667 K during the entire flight under consideration [22].

Going back then to our problem of a synergistic plane change we will consider the first phase, from the deorbit down to the conventional limit of the atmosphere, through layers in which our transitional flow model is adequate. As a usual reference condition we will assume for the initial deorbit speed variation Δu the same value which should be necessary in vacuum for a Hohmann transfer ellipse from the HEO (high earth orbit) to the LEO (low earth orbit). With this in mind we assume an altitude at HEO $H_{\mathrm{HEO}} = 200$ km and $\Delta u / u_{\mathrm{HEO}} = -0.0038$. These two values for the Hohmann transfer would lead to $H_{\mathrm{LEO}} = 105$ km.

We will not report all the results relative to the various aspects of the particular manoeuvre considered here but will focus our attention instead on the heat transfer. Figures 15 and 16 show the mean heat transfer rate ($\dot{h}$) as a function of the altitude after imposing different conditions on the angles of attack, and after assuming the standard maximum temperature limitation. For each case represented the descent is performed in such a way as to have minimum consumption, minimum heat transfer rate and maximum aerodynamic efficiency. An immediate comparison of the results for the PLV in Figure 15 with those for the caret wing in Figure 16 confirms that the heat transfer at the caret surfaces must be lower than in the case of the PLV in order not to exceed the T_W limitation, in the range of altitudes considered. The higher efficiency of the caret wing is paid in terms of a greater heat transfer. Moreover, in each case, a descent at maximum efficiency presents greater heating rates as far as the minimum fuel consumption is concerned.

We also show in Figure 17 the distribution of the local heat transfer coefficient at an altitude of 130 km and at an incidence of minimum total heat transfer for the PLV. For completion we report that the value of $c_{h_{\max}}$ for the two spacecraft at the same altitude $H = 130$ km, when each is at the incidence of minimum total heating, is equal to 0.45.

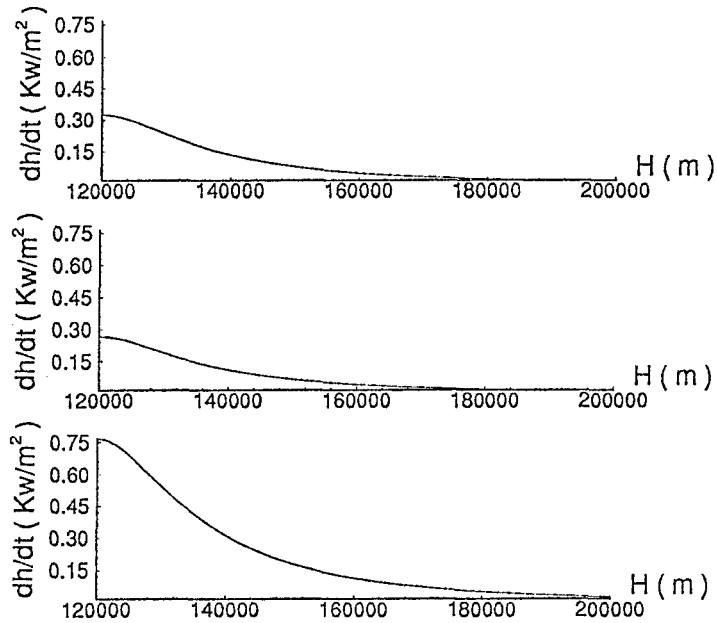

Fig. 15. Aeroassisted orbit transfer of the PLV. The heat tranfer rates are (from the top) for minimum consumption, minimum heat tranfer rate and maximum aerodynamic efficiency, τ_W corresponding to $T_W = 1667$ K and T_o changing with M.

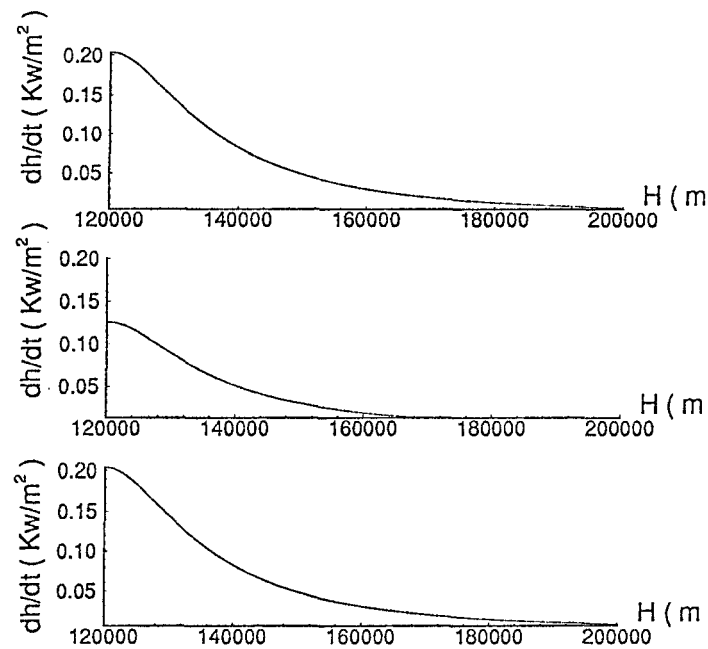

Fig. 16. Aeroassisted orbit transfer of the caret spacecraft. The heat transfer rates are (from the top) for minimum consumption, minimum heat transfer rate and maximum aerodynamic efficiency, τ_W corresponding to $T_W = 1667$ K and T_o changing with M.

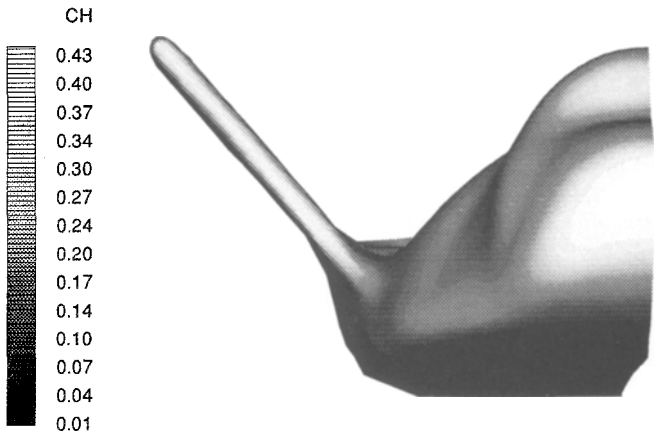

Fig. 17. Local heat transfer coefficient distribution around the PLV during an aeroassisted manoeuvre, at minimum $\dot{h}$ and $H = 130$ km.

7. Conclusion

This paper has been devoted to an evaluation of the aero-thermodynamic effects on the flight of a lifting spacecraft at very high altitudes. It was shown that, even above the usually assumed limit of the atmosphere: (i) the aerodynamic moments play a definite role in the stability of the vehicle; (ii) the heat transfer rates can be sizeable and can therefore significantly influence the time history of aeroassisted manoeuvres. The analytical expression of the gas-surface interaction model in the transitional regime in connection with a numerical solver of the motion equations proved to be very effective in simulating the high altitude trajectories of a lifting vehicle.

Acknowledgement

This work was partially supported by the Italian Space Agency through Contract No. 144SS.

References

1. Moss, J.N., 'Enhancements and applications of DSMC for hypersonic rarefied flows', in Beylich, A.E. (Ed.), *Rarefied Gasdynamics* V.C.H., Weinhiem, 1991, pp. 643–654.
2. Bird, G.A., 'Efficiency and discrepancy in the direct simulation methods', in Beylich, A.E. (Ed.), *Rarefied Gasdynamics* V.C.H., Weinhiem, 1991, pp. 655–662.
3. Kleber, P., 'Low earth orbit environment for research in space', *Earth Space Rev.* **1**, 1992, pp. 19–25.
4. Etkin, B., *Dynamics of Atmospheric Flight*, J. Wiley, New York, 1972.
5. de Divitiis, N. and de Socio, L.M., 'Vehicle aerodynamics in the transition regime', presented at the 18th *Rarefied Gasdynamics Symposium*, Vancouver, 1992.
6. Etkin, B., 'Longitudinal dynamics of a lifting vehicle in orbital flight', *J. Aerospace Sciences*, **28**(10) (1961) 779–788.
7. de Matteis, G. and de Socio, L.M., 'Stability of a tethered satellite subjected to stochastic forces', *Acta Astronautica*, **25**(2) (1991) 61–66.
8. Legge, H., 'Force and heat transfer measurements on a disc at 45°–90° angle of attack in free jet using Ar, He, N_2, H_2 as test gases', *DFVLR Rept. no. IB222–89A07*, 1989.
9. Naidu, D.S., 'Orbital plane change manoeuver with aerocruise', *AIAA Paper 91–0054*, 1991.
10. U.S. Standard Atmosphere, N.O.A.A., N.A.S.A.,U.S.A.F., Washington DC, 1976.
11. Powell, R.W. and Cruz, C.I., 'Guidance and control analysis of the entry of a lifting body personnel launch vehicle', *AIAA Paper 91–0055*, 1991.

12. Lewis, M.J. and McRonald, A.D., 'The design of hypersonic waveriders for aeroassisted interplanetary trajectories', *AIAA Paper 91-0053*, 1991.
13. Anderson, J.D., Ferguson, F. and Lewis, M.J., 'Hypersonic waveriders for high altitude applications', *AIAA Paper 91–0530*, 1991.
14. Antonov, S.G., Ivanov, M.S., Kashkovski, A.V. and Christolinov, V.G., *Influence of Atmospheric Rarefaction on Aerodynamic Characteristics of Flying Vehicles in Rarefied Gasdynamics*, in Beylich, A.E. (Ed.), Rarefied Gasdynamics V.C.H., Weinhiem, 1991, pp. 522–530.
15. Potter, J.L., 'Transitional hypervelocity aerodynamic simulation and scaling in light of recent flight data', *AIAA Paper 85–37661*, 1985.
16. Potter, J.L., 'Procedure for estimating aerodynamics of three dimensional bodies in transitional flow', *Progr. in Aeronautics and Astronautics*, **18** (1990) 484–492.
17. Cruz, C. and Wilhite, A., 'Prediction of high speed aerodynamic characteristics using the aerodynamic preliminary analysis system', *AIAA Paper 89–2173*, 1989.
18. Perminov, V.D., Gorelov, S.L., Freedlender, O.G. and Khmelnitski, A.A., 'Approximate aerodynamic analysis for complicated bodies in rarefied gas flow', in Beylich, A.E. (Ed.), *Rarefied Gasdynamics*, V.C.H., Weinhiem, 1991, pp. 554–561.
19. Cheng, H.K., Wong, E.Y. and Hoover, L.H., 'Flat plate at incidence as a waverider in rarefied hypersonic flow', *1st International Hypersonic Waverider Symposium*, University of Maryland, 1990.
20. Walberg, G.D., 'A survey of aeroassisted orbital transfer', *J. Spacecraft and Rockets*, **22** (1985) 3–18.
21. Lees, L., 'Laminar heat transfer over blunt nosed bodies at hypersonic flight speed', *Jet Propulsion*, **26** (1956) 259–269.
22. Ikawa, H. and Rudiger, T.F., 'Synergetic manoeuver of winged spacecraft for orbital plane change', *J. of Spacecraft and Rockets*, **19** (1982) 513–520.